

Changes in satellite retrievals of atmospheric composition over eastern China during the 2020 COVID-19 lockdowns

Robert D. Field^{1,2}, Jonathan E. Hickman¹, Igor V. Geogdzhayev^{1,2}, Kostas Tsigaridis^{1,3}, Susanne E. Bauer¹

¹NASA Goddard Institute for Space Studies, 2880 Broadway, New York, NY, USA, 10025

²Dept. of Applied Physics and Applied Mathematics, Columbia University 2880 Broadway, New York, NY, USA, 10025

³Center for Climate Systems Research, Columbia University, 2880 Broadway, New York, NY, USA, 10025

Correspondence to: Robert D. Field (robert.field@columbia.edu)

Abstract. We examined daily Level-3 satellite retrievals of AIRS CO, OMI SO₂ and NO₂, and MODIS AOD over eastern China to understand how COVID-19 lockdowns affected atmospheric composition. Changes in 2020 were strongly dependent on the choice of background period since 2005 and whether trends in atmospheric composition were accounted for. Over central east China during the January 23 - April 8 lockdown window, CO in 2020 was between 3% and 12% lower than average depending on the background period. ~~2020 CO was, but not consistently less than expected from trends over different periods beginning between 2005 and 2016 and ending in 2019 but was 3-4% lower than the background mean during the 2017-2019 period when CO changes had flattened.~~ Similarly for AOD, 2020 was between 14% and 30% lower than averages ~~beginning in 2005, but not distinct from what would be expected from trends beginning after 2008~~ and 14-17% lower compared to ~~different background means beginning in 2016.~~ NO₂ in 2020 was between 30% and 43% lower than the mean over different background periods and between 17% and 33% lower than what would be expected for trends beginning later than 2011. ~~Relative to the 2016-2019 period when NO₂ had flattened, 2020 was 30-33% lower.~~ Over southern China, 2020 NO₂ was between ~~2323% and 3227% lower than the mean, and between 14% and 29% lower than would be expected from different trends~~ ~~different background means beginning in 2013, the beginning of a period of persistently lower NO₂.~~ CO over southern China was significantly higher ~~in 2020~~ than what would be expected, which we suggest was partly because of an active fire season in neighbouring countries. Over central east and southern China, ~~2020~~ SO₂ was higher than expected, but this depended strongly on how daily regional values were calculated from individual retrievals ~~and reflects background values approaching the retrieval detection limit.~~ Future work over China, or other regions, needs to take into account the sensitivity of differences in 2020 to different background periods and trends in order to separate the effects of COVID-19 on air quality from previously occurring changes, or from variability in other sources.

1 Introduction

In an effort to control the spread of COVID-19, the Chinese government implemented a range of restrictions on movement. These led to reductions in industrial and other work related and personal activities starting January 23, 2020 in Wuhan, Hubei province, then extending to other cities and regions in the days that followed. On April 8, 2020, Wuhan was the last city to re-open after a complete lockdown that prevented most people from leaving their homes. These measures have been linked to changes in air quality. A network of surface monitoring stations in northern China observed 35% decreases in PM_{2.5} and 60% decreases in NO₂ concentrations during January 29

39 through February 29, as compared to the preceding three weeks; CO and SO₂ also declined (Shi and Brasseur,
40 2020). In and around Wuhan, decreases of NO₂ and PM_{2.5} were similar to regional changes, but there was a slight
41 increase in SO₂ concentrations (Shi and Brasseur, 2020). Observations by the Tropospheric Monitoring Instrument
42 (TROPOMI) showed large decreases in tropospheric NO₂ column densities over Chinese cities, on the order of
43 40% for February 11 to March 24 2020 compared to the same period in 2019, ranging from roughly 25% for cities
44 not affected by lockdown to 60% for Wuhan and Xi'an (Bauwens et al., 2020). Prospective simulations suggested
45 that meteorology may limit the effect of reduced emissions on PM_{2.5} concentrations, with Chinese cities
46 experiencing less than 20% reductions (Wang et al., 2020).

47

48 The goal of our study was to consider these changes against pollution trends in China using NASA Earth
49 Observing System data by combining several products to give a holistic view covering several emission sectors
50 that are responsible for the observed changes. Over the last 2 to 3 decades, air pollution in China appears to have
51 followed the pattern described by the Environmental Kuznets Curve (Selden and Song, 1994). This framework
52 describes a relationship in which economic growth is initially accompanied by an increase in air pollution, when
53 poverty remains widespread. But as growth continues, air pollution is expected to level off and decline as a
54 consequence of changes in social awareness of environmental degradation and the economic, political, and
55 technological capacity to limit it (Sarkodie and Strezov, 2019;Selden and Song, 1994).

56

57 Bottom-up and top-down assessments of air pollutant emissions and concentrations suggest that China has
58 followed this pattern during the era of satellite monitoring of atmospheric composition, with concentrations of
59 SO₂, NO₂, CO, and aerosol optical depth (AOD) mostly exhibiting marked and steady declines over the last
60 decade. In the case of NO₂, multi-instrument analyses, which extend the observational record beyond the lifetime
61 of a single instrument, depict a consistent regional picture of NO₂ trends in China since 1996 (Geddes et al.,
62 2016;Georgoulias et al., 2019;Wang and Wang, 2020;Xu et al., 2020). Column totals show an increasing trend
63 during the first part of the satellite record, but this trend is reversed sometime between 2010 and 2014 (Georgoulias
64 et al., 2019;Krotkov et al., 2016;Lin et al., 2019;Xu et al., 2020;Si et al., 2019;Shah et al., 2020). The trend reversal
65 has been attributed to a combination of emission control measures (Zheng et al., 2018a) and variations in economic
66 growth (Krotkov et al., 2016).

67

68 Bottom-up estimates suggest that SO₂ emissions peaked earlier, with declines starting around 2005, primarily as
69 a result of power and industrial pollution control measures as well as the elimination of small industrial boilers
70 (Sun et al., 2018;Zheng et al., 2018b). An earlier peak in SO₂ emissions is consistent with observations by multiple
71 satellite instruments, which revealed declines in SO₂ column densities since 2005 (Fioletov et al., 2016;Krotkov
72 et al., 2016;Wang and Wang, 2020;Zhang et al., 2017;Si et al., 2019).

73

74 AOD retrievals from the Along Track Scanning Radiometer instruments show a steady increase over southeastern
75 China from 1995 to 2005 (Sogacheva et al., 2020), and a decline since 2005 in the MODIS AOD (He et al., 2019).
76 The AOD peak has been argued to match either the ~2011 peak in NO₂ (Zheng et al., 2018b;Xie et al., 2019), the
77 ~2005 peak of SO₂, or to have occurred at some point in between (Ma et al., 2016), with more rapid decreases in
78 AOD after 2011 (Lin et al., 2018). The recent decrease in AOD is also seen in VIIRS retrievals (Sogacheva et al.,

79 2020). Most mitigation of direct PM_{2.5} emissions since 2010 was by industry, with residential emissions also
80 decreasing substantially (Zheng et al., 2018b). The decline in SO₂ emissions also exerted an important influence,
81 with the sulfate concentration of PM_{2.5} decreasing substantially between 2013 and 2017 (Shao et al., 2018),
82 reflecting the negative trend in SO₂ emissions.

83
84 The peak in concentrations of CO, which has an atmospheric lifetime ranging from weeks to months, is less easily
85 identified. Some studies suggest that trends have been negative potentially throughout the 21st century (Han et al.,
86 2018;Strode et al., 2016;Wang et al., 2018;Yumimoto et al., 2014;Zheng et al., 2018a), but others suggest that
87 emissions and/or column densities were increasing or flat during at least the first decade of the century (Sun et
88 al., 2018;Zhao et al., 2013;Zhao et al., 2012). The negative trend has been attributed largely to reductions in
89 emissions from industrial activity, as well as from residential and transportation sectors (Zheng et al.,
90 2018a;Zheng et al., 2018b).

91
92 In addition to these long-term trends, a number of air pollutants also exhibit strong seasonal variation in China.
93 Anthropogenic emissions of CO, SO₂, and PM_{2.5} are highest in winter, reflecting large variation in emissions from
94 the residential sector and, in the case of CO, increased emissions associated with cold-start processes in the
95 transportation sector (Li et al., 2017). Outflow of CO and AOD has a spring maximum, resulting from transport
96 of pollution, dust, and boreal biomass burning emissions (Han et al., 2018;Luan and Jaegle, 2013).

97
98 Changes in pollution over China have also come from short-term interventions. To improve air quality for the
99 2008 summer Olympics—a time when emissions in China were high and still increasing—the Chinese
100 government imposed a series of strict emissions control measures from July through September 21, 2008, which
101 were qualitatively similar to the emissions reductions expected to have accompanied the COVID-19 lockdown
102 (UNEP, 2009). As a result, NO₂ concentrations over Beijing were estimated to have declined by between 40%
103 and 60% based on satellite observations, with substantial but smaller reductions in surrounding cities often on the
104 order of 20% to 30% compared to previous years (Mijling et al., 2009;Witte et al., 2009). Regional reductions of
105 SO₂ and CO during the months of the games were estimated to be 13% and 19%, respectively (Witte et al., 2009).
106 These results are broadly consistent with on-road observations (Wang et al., 2009), but larger than some surface
107 observations comparing concentrations before and after the emission control measures were implemented (Wang
108 et al., 2010).

109
110 The COVID-related lockdowns provide a similar natural experiment to the 2008 Beijing Olympics but on the
111 other side of the Kuznets curve. The fact that the lockdowns occurred during years of decreasing air pollution
112 needs to be taken into account in attributing changes in atmospheric composition to COVID-19 lockdowns,
113 independent of the long-term trend. Following Chen et al.'s (2020) analysis of air quality improvements on
114 mortality which controlled for changes in air quality since 2016, in this study we determine whether changes in
115 2020 in satellite retrievals of CO, SO₂, NO₂ and AOD departed significantly from the expected declines associated
116 with the long-term decreases in concentrations resulting from pollution controls and technological change.

117 **2 Data and methods**

118 We used daily Level-3 (L3) retrievals from four different instruments on three different NASA Earth Observing
119 System satellites. The Atmospheric Infrared Sounder (AIRS) instrument aboard NASA's Aqua satellite is a 2300-
120 channel infrared grating spectrometer in a sun-synchronous orbit with northward equator crossing time of 1:30
121 PM. AIRS carbon monoxide (CO) profiles are retrieved with horizontal resolution of 45 km at nadir, in a swath
122 of width 30 fields-of-view or about 1600 km. The retrieval uses a cloud-clearing methodology providing CO with
123 sensitivity that peaks around 500 hPa, with ~0.8-1.2 degrees-of-freedom-of-signal for 50-70% of scenes. More
124 sampling and higher information content is obtained in clear scenes (Warner et al., 2013). We used the daily
125 version 6 (AIRS3STD.006) product.

126

127 The Ozone Monitoring Instrument (OMI) aboard NASA's Aura satellite was launched in July 2004, and has a
128 local equator-crossing time of roughly 13:45. OMI is a nadir-viewing spectrometer, which measures solar
129 backscatter in the UV-visible range (Krotkov, 2013). We used NASA's L3 tropospheric NO₂ column density
130 Standard Product v3 (OMNO2d_003), and the OMI Principal Components Analysis Planetary Boundary Layer
131 (PBL) SO₂ product (OMSO2e_003), which grid retrievals to 0.25° resolution (Krotkov et al., 2017; Li et al., 2013).
132 Both products are cloud-screened; only pixels that are at least 70% cloud-free are included in the NO₂ product,
133 and those that are at least 80% cloud-free are included in the SO₂ product. The NO₂ product relies on air mass
134 factors (AMFs) calculated with the assistance of an atmospheric chemical transport model and are sensitive to
135 model representations of emission, chemistry, and transport data. Instead of AMFs, the SO₂ product uses
136 spectrally-dependent SO₂ Jacobians, but can be interpreted as having a fixed AMF that is representative of
137 summertime conditions. We applied basic transient SO₂ plume filtering, excluding retrievals with SO₂ > 15 DU
138 (Wang and Wang, 2020).

139

140 Because our trend analysis uses a seasonal mean as the response variable, we assume that random errors cancel
141 out, leaving only systematic errors, which do not contribute to uncertainty in the trend analysis. Systematic errors
142 in the OMI NO₂ product have an uncertainty of 20% (McLinden et al., 2014) and are associated with AMFs and
143 tropospheric vertical column contents. The OMI NO₂ products use an implicit aerosol correction to account for
144 the optical effects of aerosols, but retrievals can be biased when aerosol loading is extreme (Castellanos et al.,
145 2015). Under these conditions, the OMI NO₂ retrieval is biased low by roughly 20 to 40% (Chimot et al., 2016).
146 Note that any aerosol-related error would have the potential effect of underestimating the magnitude of decreases
147 in NO₂ column densities when comparing 2020 to previous years. Additional bias in the NO₂ product may be
148 introduced due to the reliance on nearly cloud-free pixels, in which greater sunlight may induce higher
149 photochemical rates. For example, the current NO₂ product is biased roughly 30% low over the Canadian oil sands
150 (McLinden et al., 2014). The level-2 OMI- NO₂ product has been validated against in situ and surface-based
151 observations showing good agreement (Lamsal et al., 2014). The use of fixed Jacobians in the SO₂ product
152 introduces systematic errors of 50 to 100% for cloud-free observations (Krotkov et al., 2016).

153

154 Starting in 2007, the quality of level 1B radiance data for some OMI viewing directions has been affected, known
155 as the row anomaly. The L3 products used here exclude all pixels affected by the row anomaly from each
156 observation, but the locations of the row anomaly pixels were dynamic between 2007 and 2011, which could

157 affect any comparisons including those years. Since 2011, the pixels affected by the row anomaly problem are the
158 same, so comparisons for data only since 2011 are not affected by changes in the row anomaly.

159

160 Moderate Resolution Imaging Spectroradiometer (MODIS) sensors observe the Earth from polar orbit, from Terra
161 satellite since 2000 and from Aqua since mid 2002. In this study we use MODIS-derived AOD at 550nm obtained
162 by merging Dark Target and Deep Blue retrievals (Sayer et al., 2014). Specifically, we use the
163 `Deep_Blue_Aerosol_Optical_Depth_550_Land_Mean` field over land and the over ocean
164 `AOD_550_Dark_Target_Deep_Blue_Combined_Mean` the from Collection 6.1 L3 Gridded products MYD08 and
165 MOD08 (Hubanks et al., 2019), though very few retrievals over ocean are included in our analysis. L3 values are
166 computed on $1^\circ \times 1^\circ$ spatial grid from L2 AOD products with resolution of 10x10 km. Over land 66% of MODIS-
167 retrieved Dark-target AOD values were shown to be $\pm 0.05 \pm 0.15 * \text{AOD}$ AERONET-observed values, with high
168 correlation ($R = 0.9$) (Levy et al., 2010). Around 78% of the Deep Blue retrievals are within the expected error
169 range of $\pm 0.05 \pm 0.20 * \text{AOD}$ (Sayer et al., 2013). MODIS AOD data have been extensively used by the modeling
170 and remote sensing scientific communities and inter-compared with a wide range of satellite AOD products (see
171 Schutgens et al. (2020) and references therein).

172

173 We analyzed these retrievals over two large regions (Fig. 1). Central east China was comprised of Shaanxi, Hubei,
174 Anhui, Jiangsu, Shanxi, Henan, Hebei, Shandong, Beijing, and Tianjin provinces. Southern China was comprised
175 of Guizhou, Guangxi, Hunan, Jiangxi, Guangdong, Fujian and Zhejiang provinces. Daily mean quantities were
176 calculated across all valid retrievals falling within the provinces comprising the regions. For the OMI NO₂
177 columns, individual retrievals were weighted by the L3 ‘Weight’ field, which is proportional to the fraction of the
178 grid cell with higher-quality retrievals, identified as those have less than 30% cloud fraction and not affected by
179 the row anomaly problem. We also calculated the daily value from the median of all retrievals, to understand
180 whether individual high values (mainly SO₂) had any effect on the significance of trends or differences between
181 2020 and different background periods. Monthly averages were calculated from the daily regional averages, with
182 each day weighted in the monthly average by the number of valid retrievals so as to not overrepresent days with
183 little satellite coverage or significant cloud cover. The monthly data were used to visually identify COVID-19
184 related changes against background seasonality and trends since 2005.

185

186 We examined the difference in the distribution of daily data during the 2020 January 23 to April 8 lockdown
187 period to the same period during previous years since 2005. We compared 2020 to 2019, to different background
188 periods, and to the expected value for 2020 estimated from trends over different background periods. ~~We tested~~
189 ~~the significance of these differences using bootstrap resampling (Efron and Gong, 1983) with a resampling size~~
190 ~~of 2000.~~ Given the uneven nature of uncertainty and uneven nature of trends over changes in atmospheric
191 composition over different parts of China ~~from identified in~~ previous studies, background periods were defined
192 for each possible starting year between 2005 and 2018 with each ending in 2019. Retrieved quantities in 2020
193 were compared to the background means over each period and to the value expected for 2020 estimated from the
194 linear trend over each period. ~~we identified the start of existing long-term trends for each species by conducting~~
195 ~~linear regressions of the change in the four quantities over time for possible start years of 2005 to 2018. Each~~
196 ~~trend was estimated from the start year in this range until 2019.~~

197 We tested the significance of these differences using bootstrap resampling (Efron and Gong, 1983) with a
198 resampling size of 2000.

199
200 We also considered how the analysis depended on how the lockdown period was defined. Emissions and pollution
201 can decrease during the Chinese New Year holidays (Chen et al., 2020), which started as early as January 23 in
202 2012 and as late as February 19 in 2015, complicating COVID-19 related analyses of atmospheric composition
203 over China (Bauwens et al., 2020;Chen et al., 2020). The timing and extent of lockdowns also varied between
204 provinces and we assume that ‘slowdowns’ could have happened before or after stricter, official lockdowns. For
205 example, ground and air transportation remaining below lockdown levels nationally at least through April 14,
206 2020 (International Energy Agency, 2020). Excluding the holiday period from all years is a straightforward
207 approach to excluding any New Year holiday effects but will exclude simultaneous lockdown effects during the
208 initial, and presumably most strict, stages of the lockdown. Rather than specifying different combinations of New
209 Year holiday period and provincial-level lockdown timing, we used January 23-April 8 as our baseline period
210 (which will include all holiday periods since 2005), but examined the sensitivity of the statistics to the length of
211 the lockdown period, namely a longer lockdown period beginning one week earlier and one week later, and a
212 shorter lockdown period for February only. In interpreting the data, we put more confidence in 2020 differences
213 that were insensitive to these choices.

214 **3 Results**

215 **3.1 Regional patterns and seasonality**

216 Figure 2 shows the 2020 –2019 differences over China during the January 23-April 8 lockdown period
217 for the four satellite-retrieved quantities. There were decreases of 5-10 ppbv in AIRS CO over central east China
218 (Fig. 2a) and increases of 20-25 ppbv over southern China in 2020 compared to 2019. The increase in southern
219 China is adjacent to a stronger positive CO anomaly over the upper Mekong regions of Myanmar, Thailand and
220 Laos. There were no coherent regional changes in OMI SO₂ (Fig. 2b), but rather smaller localized difference of
221 either sign. There were decreases in NO₂ (Fig. 2c) across central east China exceeding 8×10^{15} molec cm⁻²
222 coincident with the weaker decrease in CO. Over southern China, there were comparable differences over
223 Guangdong province, with smaller differences elsewhere. There was a decrease in MODIS AOD (Fig. 2d) in
224 central-east China coincident with the decreases in CO and NO₂, but smaller in magnitude. There was a region of
225 higher AOD in and northeast of the upper Mekong region coincident with the CO increase, both presumably
226 because of biomass burning.

227
228 To put the 2020/2019 difference maps in a longer-term and seasonal context, Figure 3 shows monthly
229 averages of the four retrieved quantities over central east China since 2005. There are seasonal CO peaks in
230 March-April, June and September, with the minima usually in November and December (Figure 3a).
231 There has been a decrease since 2005 in CO. The seasonal decrease from January to February in 2020 is similar
232 to that which has occurred occasionally before, but the CO during February and March 2020 was the lowest for
233 that time of the year since 2005. By April, CO had returned to levels typical of 2015-2019. The main
234 characteristics of the monthly SO₂ over the region are that it has decreased since 2005 (Figure 3b), and

235 that early 2020 SO₂ was within the range of recent levels. There is a strong seasonal NO₂ cycle (Figure 3Figure
236 3c), with a July-August minimum, and December-January peak, which has been attributed to increased heating
237 needs (Yu et al., 2017;Si et al., 2019) and longer chemical lifetime owing to lower OH and RO₂ (Shah et al.,
238 2020). NO₂ has also decreased since 2011, and during most years, there is a departure from a smooth seasonal
239 cycle in January and February associated with the Chinese New Year holiday period. January and February 2020
240 NO₂ was considerably lower than previous years, increased during March, and had recovered to typical, recent
241 levels by April. AOD has consistent seasonal peaks in summer which have been attributed to hygroscopic growth
242 and agricultural residue burning (Filonchuk et al., 2019), but had less regular seasonality otherwise, and has
243 decreased since 2011. AOD during February and particularly March of 2020 were lower than recent years, but
244 during which time there was considerable variability in the monthly data.

245

246 Figure 4Figure-4 shows the four retrieved quantities over southern China. There is a springtime maximum in CO
247 (Fig. 4a), a less regular maximum during September-January, and an annual minimum in July. The range of CO
248 is similar to central east China. CO over the last 5 years is lower than earlier in the record, and early 2020 CO was
249 higher than recent years. SO₂ (Fig. 4b) is lower than central east China and any seasonal cycle is also hard to
250 identify. The high June 2011 values are due to the Nabro eruption in Ethiopia (Fromm et al., 2014) which is still
251 apparent in the time series despite excluding individual SO₂ retrievals that are greater than 15 DU, and are due to
252 a combination of higher overall background values and individual retrievals with very high (> 10 DU) SO₂. NO₂
253 (Fig. 4c) is lower than over central east China, but both regions share a similar seasonality. NO₂ during January-
254 April 2020 was slightly lower than in 2019. AOD (Fig. 4d) has weak seasonal peaks in October, March and June,
255 has decreased since 2011, and 2020 fell within the range of 2015-2019.

256

257 3.2 Central east China

258 Figure 5 shows the CO, SO₂, NO₂ and AOD for January 23 – April 8 of each year over central east China as box
259 and whisker plots with the median, interquartile range and 2.5th and 97.5th percentiles over all daily mean data as
260 horizontal lines and the mean shown by the black dot. The associated statistics comparing 2020 and 2019 are
261 provided in Table 1, and comparing 2020 to longer background periods with and without trends accounted for as
262 supplementary Tables S1-S4. The AIRS CO is shown in Figure 5a. The variation during January 23 – April 8 of
263 each year is due to weather-related factors and observational error. The mean CO of 133.5 ppbv in 2020 was 3.2%
264 less than the 2019 mean of 137.9 ppbv, which was only marginally significant, having a 95% confidence interval
265 (-6.3% - 0.1%) close to spanning 0. During years prior, there were increases and decreases in CO from year to
266 year, but an overall decreasing trend since 2005. To quantify if the 2020 departure was significant against this
267 background, we compared the distribution of observed 2020 CO to the background average and to that which
268 might be expected given any trends over the background period. Because there was no obvious starting year for
269 the background period, we considered different periods starting in each year between 2005 and 2018 and ending
270 in 2019 (Fig. 6a, Table S1). The difference between 2020 and the background depended strongly on the starting
271 year of the background period, ranging from -11.5% lower than the 2005-2019 mean to -3.1% lower than over
272 2018-2019, but all were statistically significant. Significant trends over years beginning between 2005 and 2016
273 (shown in Fig. 6a by the red line and shading) ranged between -1.5 ppbv yr⁻¹ when starting in 2013 to -3.6 ppbv

274 yr⁻¹ if starting in 2016. The uncertainty in the trends increased for trends over shorter periods, and were,
275 unsurprisingly, insignificant by 2017, with the 95% confidence intervals of the trends spanning 0. The differences
276 between the observed 2020 mean and the value predicted from the trend (magenta line) varied inversely with the
277 trend and was always negative, but, except for 2009, had 95% confidence intervals (magenta shading) spanning
278 0, and therefore were not considered significant. For CO therefore, 2020 was significantly lower than the
279 background period mean but not consistently lower than predicted given the decreasing trend during the
280 background period, no matter how this period was defined. Results were similar for CO analysed closer to the
281 surface at 850 hPa (not shown), but where the retrieval has less sensitivity.

282
283 OMI SO₂ (Fig. 5b) fluctuated over 2005 to 2011 and declined steadily afterward during which variation also
284 declined, becoming narrower to a degree not seen in the CO. The 2020 mean of 0.057 was 95% higher than the
285 2019 mean of 0.031, but with a wide 95% confidence interval (15% - 250%). For different background periods
286 (Table S2), 2020 SO₂ ranged from 83% less than the 2005-2019 mean to 30% less than the 2016-2019 mean, with
287 insignificant differences compared to more recent periods. Trends varied significantly from to -0.03 yr⁻¹ over
288 2005-2019 to -0.06 DU yr⁻¹ over 2012-2019 (Fig. 6b), during which the trend could explain a maximum of 32%
289 of the variation in the data. For periods starting in 2007 and after, the observed 2020 mean was significantly higher
290 than predicted. Relative to the value predicted from the 2012-2019 trend of -0.06, the observed 2020 SO₂ was
291 200% higher; the large percent difference reflects a predicted value close to zero, and we note that the retrieved
292 SO₂ can be negative for individual values and averages (Li et al., 2013; Wang and Wang 2020). The observed
293 2020 SO₂ was much higher than expected from trends calculated over 2016-2019 when SO₂ was flat and with less
294 variability, but the low SO₂ approaching the detection limit over this period make these estimates not particularly
295 meaningful. Furthermore~~While this difference was significant~~, the change in 2020 SO₂ was strongly dependent
296 on whether daily values were calculated from the mean or median of individual values over the region. For most
297 background periods (Figure S1b), the trends in the median values were still negative until 2015, but 2020 was
298 only 8.4% higher than predicted from the 2012-2019 trend and not significantly different from expected for trends
299 beginning later. This likely reflects the greater influence of high individual retrieval values on the daily mean
300 value compared to the median, even after the basic filtering of transient SO₂ plumes.

301
302 OMI NO₂ (Fig. 5c) increased from 2005 to 2011 and decreased thereafter with an apparent flattening since 2016.
303 The 2020 mean NO₂ of 6.5x10¹⁵ molec cm⁻² was 32% less than the 2019 mean of 9.6 x10¹⁵ molec cm⁻²; the
304 pronounced regional difference between 2020 and 2019 (Fig. 2c, [Fig. 5c](#)) in part reflects a 2019 uptick from 2018.
305 For different background periods (Table S3), 2020 NO₂ ranged from 43.3% less than the 2010-2019 mean to 30%
306 less than the 2018-2019 mean, with all differences significant. Trends were negative and significant for starting
307 years between 2007 and 2015 (Fig. 6c) with the strongest trend of -0.7 5x10¹⁵ molec cm⁻² yr⁻¹ for the period
308 beginning in 2011. 2020 NO₂ was significantly less than the predicted value for all background periods but varied
309 from 16.8% less than predicted from the 2011-2019 trend to 27.1% less than predicted from the 2015-2019 trend,
310 the last period when there was a significant, although weak, decrease.

311
312 MODIS AOD (Fig. 5d) was flat or slightly increasing from 2005 to 2011, decreasing thereafter and with a
313 flattening since 2016 similar to SO₂ and NO₂. The 2020 mean AOD of 0.41 was 14% less than the 2019 mean of

314 0.48, but this was not significant. For different background periods (Table S4), 2020 AOD ranged from 30.2%
315 less than the 2007-2019 mean to 14.2% less than the 2018-2019 mean, with confidence intervals for the
316 differences becoming closer to spanning 0 for more recent periods. Trends were negative and significant for
317 starting years between 2005 and 2014 (Fig. 6d), with the strongest decrease of 0.04 yr⁻¹ over the 2012-2019 period.
318 There was no significant difference between the observed and predicted 2020 mean for periods beginning in 2008
319 and later, when the trends were strongest, and which approached 0 after 2014.

320 3.3 Southern China

321 Figure 7 shows the distribution of daily CO, SO₂, NO₂ and AOD for January 23-April 8 of each year over southern
322 China. The associated statistics comparing 2020 and 2019 are provided in Table 2. AIRS CO (Fig. 7a) in 2020
323 was 144.7 ppbv, 13% higher than the 2019 mean of 128.5 ppbv which can be seen in an upward shift in the
324 distribution of the box plot. 2020 CO was between 4.4% and 8.8% greater than the background mean for periods
325 starting after 2014 (Table S5), but not significantly different otherwise. CO decreased significantly for periods
326 starting between 2005 and 2016 (Fig. 8a). When these trends are taken into account, 2020 CO was between 11.2%
327 and 18.7% greater than predicted, and in all cases were significant.

328
329 OMI SO₂ (Fig. 7b) fluctuated from 2005 until 2013 and flattened afterwards, driven by fewer high individual SO₂
330 values in later years, as in central east China. The 2020 mean of 0.003 DU was 116% higher than the 2019 mean
331 of -0.02 DU but also with a wide 95% confidence interval (24% - 223%). 2020 was less than the background
332 mean periods starting between 2005 and 2011 (Table S6), but not significantly different otherwise. SO₂ trends
333 were consistently negative for all periods (Fig. 8b), although not as strong as over central east China. Whether
334 2020 SO₂ was greater than predicted from trends depended more on the background period than over central east
335 China and were also not significantly different from predicted when daily values were calculated from the median
336 SO₂ of individual retrievals for any background period (Figure S2b).

337
338 OMI NO₂ (Fig. 7c) increased toward 2011 and 2012, declining after to 2005-2010 levels. The 2020 mean of
339 3.3×10^{15} molec cm⁻² was 22% less than the 2019 mean of 4.3×10^{15} molec cm⁻². For longer background periods,
340 2020 was between 22.9% and 30.6% less than the mean (Table S7), all of which were significant. NO₂ trends
341 were significantly negative ~~for periods beginning between~~ when the start of the trend was calculated using years
342 between 2007 and 2012, but not otherwise (Fig. 8c). The 2020 NO₂ mean was significantly lower than predicted,
343 except for when the trend was estimated beginning in 2011 or 2018. A two-year trend ~~is hard to~~ cannot be
344 interpreted meaningfully, especially without considering meteorological differences. ~~V~~ but visually, however, it
345 is hard to tell if the 2020 NO₂ distribution represents a COVID-related departure or a decrease comparable to
346 changes during recent previous years, unlike over central east China.

347
348 MODIS AOD (Fig. 7d) was comparable to NO₂ in its increase toward 2012, decrease thereafter and flattening
349 during more recent years. The 2020 mean AOD of 0.38 was 12% higher than the 2019 mean of 0.34, but with a
350 95% confidence interval (-7% - 34%) spanning 0. Similarly, 2020 was between 14% and 22% lower than during
351 background periods beginning from 2005 to 2012, but not for more recent periods (Table S8). The AOD trends
352 were significantly negative for all start years until 2015. The 2020 mean was between 32 and 47% higher than

353 predicted from trends for periods starting between 2010 and 2015, but ~~not otherwise~~ was not different from
354 predicted for trends starting in other years.

355

356 For both regions and all quantities, the differences between observed and predicted values for 2020 were
357 insensitive to a longer lockdown period, or to whether the bootstrap resampling was weighted by the number of
358 valid retrievals each day. For a February-only lockdown period (Figures S3 and S4), the CO trends were more
359 significant when starting in later years, but the differences between the observed and expected values remained
360 insignificant over central east China. The SO₂ trends for different periods were similar. The 2020 SO₂ differences
361 from what would be expected approached 0 for later periods but were also ~~inconsistent~~ not consistently different
362 when the median values of individual retrievals were used. Results for NO₂ were unaffected. The AOD 2020
363 difference from what would be expected was stronger and technically significant, but still with a very wide
364 confidence interval and therefore difficult to interpret. We emphasize that while a February-only lockdown period
365 is useful for comparison, it is problematic in not including the New Year's holiday periods from all previous years.

366 **4 Discussion and conclusions**

367 The degree to which the COVID-19 lockdowns in China resulted in changes in atmospheric composition depended
368 strongly on the background period and whether existing trends were taken into account. For AIRS CO over central
369 east China, the 2020 mean was 3-12% less than that over ~~lower compared to 2005-2019 and 3% lower than since~~
370 2018 ~~different background periods. Relative to mean CO concentrations during periods beginning between 2005~~
371 and 2016, there were significant decreases in CO but CO in 2020 ~~but~~ was not consistently different from what
372 would be expected ~~from trends calculated over this period given the steady decreases over different periods. These~~
373 longer-term declines in CO concentrations do appear to flatten out in recent years; assuming that the flat CO
374 during 2017-2019 would have persisted, we estimate a 3-4% reduction in CO in 2020 relative to that period.
375 ~~Similarly~~ for MODIS AOD, the 2020 mean was between 14% and 30% less than different background averages,
376 but not significantly different from what would be expected for trends beginning ~~after~~ between 2008 and 2014.
377 As with CO trends, the negative AOD trends in the region also appear to flatten in recent years. Relative to the
378 flat AOD over 2016-2019, 2020 AOD was 14-17% lower than the background mean; as with CO, this range would
379 be the more meaningful estimate of changes in 2020 if we assume that this flattening were to persist. ~~2020 SO₂~~
380 was significantly lower than background averages calculated over most periods, ranging from 83% less than over
381 2005-2019 to 30% less than over 2016-2019. Compared to the 2012-2019 period when there were no significant
382 SO₂ increases, 2020 SO₂ was 200% greater than what would be expected based on a trend starting in 2021, but
383 only 8% greater when the median value of daily retrievals was used, and not significantly different from expected
384 relative to the trends beginning later than 2012. SO₂ concentrations were relatively flat from 2016-2019; when
385 using 2016 as the first year of the trend, SO₂ was significantly higher than the expected value when calculated
386 from the mean of the daily SO₂ retrievals, but not significantly different when calculated from the median. We
387 note also that analyses of SO₂ and NO₂ that include years prior to 2012 may be affected by changes in observation
388 sample size due to changes in the OMI row anomaly.

389

390 OMI NO₂ in 2020 over central east China was consistently lower than the background average and expected value
391 from the trends. There was, ~~but the latter value ranged from a~~ 17% decrease in 2020 relative to the value expected

392 ~~from for~~ a trend calculated over 2011-2019, ~~but to a 33% decrease compared to 2018 2019 during which NO₂~~
393 ~~trends had flattened~~ 30-33% decrease relative to the different background means since 2016 when the NO₂ was
394 relatively flat. Again assuming that this flattening were to persist, this latter range may be the more meaningful
395 baseline for the 2020 decrease. ~~While there were clear decreases in 2020 NO₂, this does suggest that some part of~~
396 ~~the reductions in NO₂ in 2020 could be expected independent of COVID-19 lockdowns.~~ For reference, Bauwens
397 et al. (2020) reported a ~40% drop in OMI NO₂ from 2019 to 2020 over cities affected by the lockdown using the
398 QA4ECV retrieval (Boersma et al., 2018), and a ~51% drop in NO₂ over the eight cities (Beijing, Jinan, Nanjing,
399 Qingdao, Tianjin, Wuhan, Xi'an and Zhengzhou) falling within our central east China region. Our analysis cannot
400 be compared directly because we include non-urban areas and define the lockdown period differently, but we do
401 note that NO₂ during the same period in 2019 appeared to be anomalously high relative to the previous few years,
402 which would make the decreases in 2020 appear more significant, but we can say that some of the reduction in
403 that study is possibly due to background trends in addition to COVID-19 lockdowns.

404
405 The ~~lack of any significant departure from recent trends in~~ modest decreases in CO and AOD over central east
406 China ~~was were~~ unexpected, given its high population density and level of industrial activity, lockdowns may
407 have been anticipated to lead to larger decreases. In the case of MODIS AOD, ~~the lack of an observable lockdown~~
408 ~~effect~~ these modest decreases was were possibly due to contributions from other sources unaffected by COVID-
409 19 related lockdowns, limitations in the MODIS AOD retrieval under cloudy conditions, climatological variability
410 from other sources such as mineral dust, and meteorology favourable to secondary aerosol formation which could
411 have offset lower emissions (Wang et al., 2020). The 2020 increase in SO₂ is more difficult to interpret because
412 of the discrepancies between daily values calculated from the mean or median of individual retrievals, but is
413 broadly consistent with surface observations that find no significant change in in-situ surface SO₂ over Wuhan in
414 the daily mean, and a slight increase in daytime SO₂ possibly associated with increased residential heating and
415 cooking (Shi and Brasseur, 2020).

416
417 Over southern China retrieved 2020 SO₂ was significantly lower than the background average only for periods
418 beginning between 2005 to 2011. Significant departures from expected trends were uneven ~~for when using~~ the
419 mean value of daily retrievals and absent ~~for when using~~ the median value. As with central East China, we
420 conclude that no significant changes could be robustly detected in 2020 SO₂. NO₂ in 2020 was between 23% and
421 32% less than the background average for different periods. Here, the flattening in NO₂ beginning in 2013 is easier
422 to identify than over central east China because of the much higher NO₂ during the three years prior; 2020 NO₂
423 was 23-27% less than different background means between 2013 and 2019, and between 14% and 23% less than
424 expected from trends, with insignificant differences when trends were calculated beginning in 2011 or 2018. The
425 more significant reductions in NO₂ in central east China compared to the south is presumably due the former's
426 greater population and industrialization, and consequently higher pollution levels. This is consistent with Chen et
427 al.'s (2020) detection of a larger 2020 decrease in surface NO₂ in Wuhan compared to Shanghai. Retrieved CO in
428 2020 was between 4 and 8% greater than background averages beginning in 2014, but between 11% and 19%
429 higher than what would be expected given the decreasing trends over any period. AOD in 2020 was lower than
430 background averages calculated starting with years earlier than 2012, but higher or not significantly different from

431 ~~expected for trends calculated starting in years after 2012 beginning until 2012, but higher or not significantly~~
432 ~~different from expected for trends beginning after.~~

433

434 The focus of this analysis is on whether satellite retrievals of atmospheric composition over 2020 departed
435 significantly from different background periods and expected values for 2020 when daily variability and trends
436 are accounted for, but it is useful at a preliminary stage to speculate as to how different emissions changes could
437 have contributed to 1) why NO₂ was robustly lower in 2020 over central east China compared to CO and AOD,
438 and 2) why CO and perhaps AOD were higher over southern China compared to what would be expected from
439 recent trends.

440

441 To understand why NO₂ differences over central east China were more significant than other quantities, Table 3
442 shows the emissions by sector for a representative set of constituents from the Community Emissions Data System
443 (CEDS) (Hoesly et al., 2018) over China for 2014, the most recent year available. Other bottom-up emissions
444 inventories will vary in absolute emissions amounts and their sector contributions, particularly for more recent
445 periods, but CEDS is the standard available emissions dataset available globally as a baseline for the next IPCC
446 assessment, in anticipation of assessing 2020 COVID-19 related changes to atmospheric composition in other
447 regions, and for modeling studies involving a transboundary transport component. Across all species, energy
448 production, industrial activity, transportation, residential/commercial/other (RCO), and waste disposal constitute
449 the bulk of the emissions. Based on activity data for the first quarter of 2020, energy demand across China declined
450 by 7% compared to 2019, and transportation sector activity declined by 50 to 75% in regions with lockdowns in
451 place (International Energy Agency, 2020). These sectors are direct or indirect sources of numerous pollutants,
452 including SO₂ (the precursor of sulfate aerosol), NO_x, CO, and primary anthropogenic aerosols classified broadly
453 as organic carbon (OC) and black carbon (BC). If we apply the 7% reduction in energy production and mid-point
454 62.5% reduction to transportation from the IEA, assume a 20% reduction in industrial emissions, 5% reduction in
455 waste emissions, no change in RCO (with commercial decreases offset by residential increases), this yields a 10%
456 reduction in BC, 5% reduction in OC, 14% reduction in SO₂, 14% reduction in CO and 21% reduction in NO₂.
457 The larger reduction in NO₂ relative to other emissions could partly explain why OMI NO₂ column density
458 changes over central east China were stronger than in the other retrievals.

459

460 Following Si et al.'s (2019) consideration of biomass burning as a pollution source in China alongside
461 anthropogenic sources, we considered transboundary smoke transport as a possible reason for the higher 2020 CO
462 over southern China, guided by higher CO over the Upper Mekong region in 2020 compared to 2019 (Fig. 2a)
463 and the predominant westerly flow during this time of year (Reid et al., 2013). Table 4 compares January 23-April
464 8 AIRS CO over southern China to CO emissions estimates from biomass burning from the Global Fire
465 Assimilation System (GFAS) (Kaiser et al., 2012) over the upper Mekong region (17° N to 25° N, 95° E to 105°
466 E) including parts of eastern Myanmar, northern Thailand, and northern Laos. From 2005 to 2020, variation in
467 GFAS CO over this region explained a moderate (32%) amount of variability in AIRS CO over southern China,
468 suggesting it as a non-negligible contributor to variation in CO concentration, and a contributor to higher CO
469 in 2020. This illustrates that, at a minimum, sources such as biomass burning smoke and dust that are less affected
470 by COVID-19 related measures will complicate attribution studies. To that end, modeling studies following Wang

471 et al. (2020) will be required to isolate emissions, meteorological and chemical drivers of changes in atmospheric
472 composition and their effects at a process level. With proper instrument-equivalent comparisons, modelling
473 studies will also help to identify the extent to which the lack of significant changes are due to retrieval limitations,
474 namely low sensitivity near the surface where differences would presumably be more pronounced, particularly
475 given remote emissions sources such as dust, biomass burning smoke and volcanic SO₂, which will arrive at higher
476 altitudes.

477

478 The key implication of our study is that interpreting differences in 2020 retrievals of atmospheric composition
479 depends strongly on how the background period is defined and whether trends over these periods are accounted
480 for. Not taking these into account could lead to misattribution of changes in air quality to COVID-19 lockdowns,
481 or, at a minimum, that whether differences in 2020 are significant depend on the choice of background period,
482 which is somewhat subjective. Leading up to 2020, there was an apparent flattening of decreasing trends beginning
483 earlier in the decade across the retrievals; the considerable variability in the data made identifying this flattening
484 easier in some cases than in others. We are more confident, for example, in our estimate of a 23-27% decrease in
485 2020 NO₂ over southern China relative to a flat background period than the 30-33% decrease over central East
486 China, where the recent variability was greater and the flattening less apparent. Revisiting this type of analysis in
487 the years when regional economies have fully recovered post COVID-19 will help to distinguish between further
488 decreases and flat trends and will lend themselves to using non-linear models in estimating the trends. We have
489 approached the issue by comparing data for 2020 to what would have been expected given recent trends and by
490 applying a single lockdown period to two large regions, with additional analyses to gauge the sensitivity of the
491 2020 differences to these choices. Other studies over China or elsewhere will inevitably use other approaches that
492 more explicitly account for seasonality, meteorology, and which relate changes in pollution over smaller areas
493 (e.g. single provinces or states) to region-specific lockdown measures and timing at a process level. Regardless
494 of the approach, however, it is important to consider recent trends and variability. In places where pollution has
495 decreased, not accounting for recent context could result in over-attribution of changes in pollution to COVID-
496 19. In places where pollution has increased, such as parts of South Asia, this could result in under-attribution.

497 **Code/data availability:** All code will be made available if the article is accepted for final publication. All source
498 data are publicly available.

499

500 **Competing interests:** The authors have no competing interests.

501

502 **Author contribution:** All authors conceived of the study. RF, IG and KT conducted the data analysis. RF and
503 JH prepared the manuscript with contributions from all co-authors.

504

505 **References**

- 506 Bauwens, M., Compernelle, S., Stavrakou, T., Müller, J., van Gent, J., Eskes, H., Levelt, P. F., van der A., R.,
507 Veeffkind, J. P., Vlietinck, J., Yu, H., and Zehner, C.: Impact of coronavirus outbreak on NO₂ pollution assessed using
508 TROPOMI and OMI observations, *Geophysical Research Letters*, 2, 0-3, 10.1029/2020GL087978, 2020.
- 509 Boersma, K. F., Eskes, H. J., Richter, A., De Smedt, I., Lorente, A., Beirle, S., van Geffen, J., Zara, M., Peters, E.,
510 Van Roozendael, M., Wagner, T., Maasakkers, J. D., van der A., R. J., Nightingale, J., De Rudder, A., Irie, H., Pinardi,
511 G., Lambert, J. C., and Compernelle, S. C.: Improving algorithms and uncertainty estimates for satellite NO₂
512 retrievals: results from the quality assurance for the essential climate variables (QA4ECV) project, *Atmospheric*
513 *Measurement Techniques*, 11, 6651-6678, 10.5194/amt-11-6651-2018, 2018.
- 514 Castellanos, P., Boersma, K. F., Torres, O., and de Haan, J. F.: OMI tropospheric NO₂ air mass factors over South
515 America: effects of biomass burning aerosols, *Atmospheric Measurement Techniques*, 8, 3831-3849, 10.5194/amt-8-
516 3831-2015, 2015.
- 517 Chen, K., Wang, M., Huang, C., Kinney, P. L., and Paul, A. T.: Air Pollution Reduction and Mortality Benefit during
518 the COVID-19 Outbreak in China, *Lancet Planetary Health*, 0-3, 10.1101/2020.03.23.20039842, 2020.
- 519 Chimot, J., Vlemmix, T., Veeffkind, J. P., de Haan, J. F., and Levelt, P. F.: Impact of aerosols on the OMI tropospheric
520 NO₂ retrievals over industrialized regions: how accurate is the aerosol correction of cloud-free scenes via a simple
521 cloud model?, *Atmospheric Measurement Techniques*, 9, 359-382, 10.5194/amt-9-359-2016, 2016.
- 522 Efron, B., and Gong, G.: A Leisurely Look at the Bootstrap, the Jackknife, and Cross-Validation, *American Statistician*,
523 37, 36-48, 10.2307/2685844, 1983.
- 524 Filonchyk, M., Yan, H. W., and Zhang, Z. R.: Analysis of spatial and temporal variability of aerosol optical depth
525 over China using MODIS combined Dark Target and Deep Blue product, *Theoretical and Applied Climatology*, 137,
526 2271-2288, 10.1007/s00704-018-2737-5, 2019.
- 527 Fioletov, V. E., McLinden, C. A., Krotkov, N., Li, C., Joiner, J., Theys, N., Carn, S., and Moran, M. D.: A global
528 catalogue of large SO₂ sources and emissions derived from the Ozone Monitoring Instrument, *Atmospheric Chemistry*
529 *and Physics*, 16, 11497-11519, 10.5194/acp-16-11497-2016, 2016.
- 530 Fromm, M., Kablick, G., Nedoluha, G., Carboni, E., Grainger, R., Campbell, J., and Lewis, J.: Correcting the record
531 of volcanic stratospheric aerosol impact: Nabro and Sarychev Peak, *Journal of Geophysical Research-Atmospheres*,
532 119, 10.1002/2014jd021507, 2014.
- 533 Geddes, J. A., Martin, R. V., Boys, B. L., and van Donkelaar, A.: Long-Term Trends Worldwide in Ambient NO₂
534 Concentrations Inferred from Satellite Observations, *Environmental Health Perspectives*, 124, 281-289,
535 10.1289/ehp.1409567, 2016.
- 536 Georgoulias, A. K., van der A., R. J., Stammes, P., Boersma, K. F., & Eskes, H. J.: Trends and trend reversal detection
537 in two decades of tropospheric NO₂ satellite observations, *Atmospheric Chemistry and Physics*, 19, 6269–6294,
538 <https://doi.org/10.5194/acp-2018-988>, 2019.
- 539 Han, H., Liu, J., Yuan, H. L., Jiang, F., Zhu, Y., Wu, Y., Wang, T. J., and Zhuang, B. L.: Impacts of Synoptic Weather
540 Patterns and their Persistency on Free Tropospheric Carbon Monoxide Concentrations and Outflow in Eastern China,
541 *Journal of Geophysical Research-Atmospheres*, 123, 7024-7046, 10.1029/2017jd028172, 2018.

- 542 He, Q. Q., Gu, Y. F., and Zhang, M.: Spatiotemporal patterns of aerosol optical depth throughout China from 2003 to
543 2016, *Science of the Total Environment*, 653, 23-35, 10.1016/j.scitotenv.2018.10.307, 2019.
- 544 Hoesly, R. M., Smith, S. J., Feng, L. Y., Klimont, Z., Janssens-Maenhout, G., Pitkanen, T., Seibert, J. J., Vu, L.,
545 Andres, R. J., Bolt, R. M., Bond, T. C., Dawidowski, L., Kholod, N., Kurokawa, J., Li, M., Liu, L., Lu, Z. F., Moura,
546 M. C. P., O'Rourke, P. R., and Zhang, Q.: Historical (1750-2014) anthropogenic emissions of reactive gases and
547 aerosols from the Community Emissions Data System (CEDS), *Geoscientific Model Development*, 11, 369-408,
548 10.5194/gmd-11-369-2018, 2018.
- 549 Hubanks, P., Platnick, S., King, M., and Ridgway, B.: MODIS Algorithm Theoretical Basis Document No. ATBD-
550 MOD-30 for Level-3 Global Gridded Atmosphere Products (08_D3, 08_E3, 08_M3) and Users Guide (Collection 6.0
551 & 6.1, Version 4.4, 20 Feb 2019), NASA Goddard Space Flight Center, Greenbelt, MD, 2019.
- 552 Kaiser, J. W., Heil, A., Andreae, M. O., Benedetti, A., Chubarova, N., Jones, L., Morcrette, J. J., Razinger, M., Schultz,
553 M. G., Suttie, M., and van der Werf, G. R.: Biomass burning emissions estimated with a global fire assimilation system
554 based on observed fire radiative power, *Biogeosciences*, 9, 527-554, 10.5194/bg-9-527-2012, 2012.
- 555 Krotkov, N. A.: OMI/Aura NO₂ Cloud-Screened Total and Tropospheric Column L3 Global Gridded 0.25 degree x
556 0.25 degree V3, NASA Goddard Space Flight Center, 2013.
- 557 Krotkov, N. A., McLinden, C. A., Li, C., Lamsal, L. N., Celarier, E. A., Marchenko, S. V., Swartz, W. H., Bucsela,
558 E. J., Joiner, J., Duncan, B. N., Boersma, K. F., Veefkind, J. P., Levelt, P. F., Fioletov, V. E., Dickerson, R. R., He,
559 H., Lu, Z., and Streets, D. G.: Aura OMI observations of regional SO₂ and NO₂ pollution changes from 2005 to 2015,
560 *Atmospheric Chemistry and Physics*, 16, 4605-4629, 10.5194/acp-16-4605-2016, 2016.
- 561 Krotkov, N. A., Lamsal, L. N., Celarier, E. A., Swartz, W. H., Marchenko, S. V., Bucsela, E. J., Chan, K. L., Wenig,
562 M., and Zara, M.: The version 3 OMI NO₂ standard product, *Atmospheric Measurement Techniques*, 10, 3133-3149,
563 10.5194/amt-10-3133-2017, 2017.
- 564 Lamsal, L. N., Krotkov, N. A., Celarier, E. A., Swartz, W. H., Pickering, K. E., Bucsela, E. J., Gleason, J. F., Martin,
565 R. V., Philip, S., Irie, H., Cede, A., Herman, J., Weinheimer, A., Szykman, J. J., and Knepp, T. N.: Evaluation of OMI
566 operational standard NO₂ column retrievals using in situ and surface-based NO₂ observations, *Atmospheric
567 Chemistry and Physics*, 14, 11587-11609, 10.5194/acp-14-11587-2014, 2014.
- 568 Levy, R. C., Remer, L. A., Kleidman, R. G., Mattoo, S., Ichoku, C., Kahn, R., and Eck, T. F.: Global evaluation of
569 the Collection 5 MODIS dark-target aerosol products over land, *Atmospheric Chemistry and Physics*, 10, 10399-
570 10420, 10.5194/acp-10-10399-2010, 2010.
- 571 Li, C., Joiner, J., Krotkov, N. A., and Bhartia, P. K.: A fast and sensitive new satellite SO₂ retrieval algorithm based
572 on principal component analysis: Application to the ozone monitoring instrument, *Geophysical Research Letters*, 40,
573 6314-6318, 10.1002/2013gl058134, 2013.
- 574 Li, M., Zhang, Q., Kurokawa, J., Woo, J. H., He, K. B., Lu, Z. F., Ohara, T., Song, Y., Streets, D. G., Carmichael, G.
575 R., Cheng, Y. F., Hong, C. P., Huo, H., Jiang, X. J., Kang, S. C., Liu, F., Su, H., and Zheng, B.: MIX: a mosaic Asian
576 anthropogenic emission inventory under the international collaboration framework of the MICS-Asia and HTAP,
577 *Atmospheric Chemistry and Physics*, 17, 935-963, 10.5194/acp-17-935-2017, 2017.
- 578 Lin, C. Q., Liu, G., Lau, A. K. H., Li, Y., Li, C. C., Fung, J. C. H., and Lao, X. Q.: High-resolution satellite remote
579 sensing of provincial PM 2.5 trends in China from 2001 to 2015. *Atmospheric Environment*, 180, 110-116,
580 <https://doi.org/10.1016/j.atmosenv.2018.02.045>, 2018.
- 581 Lin, N., Wang, Y. X., Zhang, Y., and Yang, K.: A large decline of tropospheric NO₂ in China observed from space
582 by SNPP OMPS, *Science of the Total Environment*, 675, 337-342, 10.1016/j.scitotenv.2019.04.090, 2019.

- 583 Luan, Y., and Jaegle, L.: Composite study of aerosol export events from East Asia and North America, *Atmospheric*
584 *Chemistry and Physics*, 13, 1221-1242, 10.5194/acp-13-1221-2013, 2013.
- 585 Ma, Z. W., Hu, X. F., Sayer, A. M., Levy, R., Zhang, Q., Xue, Y. G., Tong, S. L., Bi, J., Huang, L., and Liu, Y.:
586 *Satellite-Based Spatiotemporal Trends in PM_{2.5} Concentrations: China, 2004-2013*, *Environmental Health*
587 *Perspectives*, 124, 184-192, 10.1289/ehp.1409481, 2016.
- 588 McLinden, C. A., Fioletov, V., Boersma, K. F., Kharol, S. K., Krotkov, N., Lamsal, L., Makar, P. A., Martin, R. V.,
589 Veefkind, J. P., and Yang, K.: Improved satellite retrievals of NO₂ and SO₂ over the Canadian oil sands and
590 comparisons with surface measurements, *Atmospheric Chemistry and Physics*, 14, 3637-3656, 10.5194/acp-14-3637-
591 2014, 2014.
- 592 Mijling, B., van der A, R. J., Boersma, K. F., Van Roozendaal, M., De Smedt, I., and Kelder, H. M.: Reductions of
593 NO₂ detected from space during the 2008 Beijing Olympic Games, *Geophysical Research Letters*, 36,
594 10.1029/2009gl038943, 2009.
- 595 Reid, J. S., Hyer, E. J., Johnson, R. S., Holben, B. N., Yokelson, R. J., Zhang, J. L., Campbell, J. R., Christopher, S. A., Di
596 Girolamo, L., Giglio, L., Holz, R. E., Kearney, C., Miettinen, J., Reid, E. A., Turk, F. J., Wang, J., Xian, P., Zhao, G. Y.,
597 Balasubramanian, R., Chew, B. N., Janjai, S., Lagrosas, N., Lestari, P., Lin, N. H., Mahmud, M., Nguyen, A. X., Norris, B.,
598 Oanh, N. T. K., Oo, M., Salinas, S. V., Welton, E. J., and Liew, S. C.: Observing and understanding the Southeast Asian
599 aerosol system by remote sensing: An initial review and analysis for the Seven Southeast Asian Studies (7SEAS) program,
600 *Atmospheric Research*, 122, 403-468, 10.1016/j.atmosres.2012.06.005, 2013.
- 601
602 Sarkodie, S. A., and Strezov, V.: A review on Environmental Kuznets Curve hypothesis using bibliometric and meta-
603 analysis, *Science of the Total Environment*, 649, 128-145, 10.1016/j.scitotenv.2018.08.276, 2019.
- 604 Sayer, A. M., Hsu, N. C., Bettenhausen, C., and Jeong, M. J.: Validation and uncertainty estimates for MODIS
605 Collection 6 "Deep Blue" aerosol data, *Journal of Geophysical Research-Atmospheres*, 118, 7864-7872,
606 10.1002/jgrd.50600, 2013.
- 607 Sayer, A. M., Munchak, L. A., Hsu, N. C., Levy, R. C., Bettenhausen, C., and Jeong, M. J.: MODIS Collection 6
608 aerosol products: Comparison between Aqua's e-Deep Blue, Dark Target, and "merged" data sets, and usage
609 recommendations, *Journal of Geophysical Research-Atmospheres*, 119, 13965-13989, 10.1002/2014jd022453, 2014.
- 610 Schutgens, N., Sayer, A. M., Heckel, A., Hsu, C., Jethva, H., de Leeuw, G., Leonard, P. J. T., Levy, R. C., Lipponen,
611 A., Lyapustin, A., North, P., Popp, T., Poulson, C., Sawyer, V., Sogacheva, L., Thomas, G., Torres, O., Wang, Y.,
612 Kinne, S., Schulz, M., and Stier, P.: An AeroCom/AeroSat study: Intercomparison of Satellite AOD Datasets for
613 Aerosol Model Evaluation, *Atmos. Chem. Phys. Discuss.*, 2020, 1-43, 10.5194/acp-2019-1193, 2020.
- 614 Selden, T. M., and Song, D. Q.: Environmental Quality and Development - is there a Kuznets Curve for Air-Pollution
615 Emissions?, *Journal of Environmental Economics and Management*, 27, 147-162, 10.1006/jeem.1994.1031, 1994.
- 616 Shah, V., Jacob, D. J., Li, K., Silvern, R. F., Zhai, S. X., Liu, M. Y., Lin, J. T., and Zhang, Q.: Effect of changing NO_x
617 lifetime on the seasonality and long-term trends of satellite-observed tropospheric NO₂ columns over China,
618 *Atmospheric Chemistry and Physics*, 20, 1483-1495, 10.5194/acp-20-1483-2020, 2020.
- 619 Shao, P. Y., Tian, H. Z., Sun, Y. J., Liu, H. J., Wu, B. B., Liu, S. H., Liu, X. Y., Wu, Y. M., Liang, W. Z., Wang, Y.,
620 Gao, J. J., Xue, Y. F., Bai, X. X., Liu, W., Lin, S. M., and Hu, G. Z.: Characterizing remarkable changes of severe
621 haze events and chemical compositions in multi-size airborne particles (PM₁, PM_{2.5} and PM₁₀) from January 2013
622 to 2016-2017 winter in Beijing, China, *Atmospheric Environment*, 189, 133-144, 10.1016/j.atmosenv.2018.06.038,
623 2018.

- 624 Shi, X., and Brasseur, G. P.: The Response in Air Quality to the Reduction of Chinese Economic Activities during the
625 COVID-19 Outbreak, *Geophysical Research Letters*, 0-1, 10.1029/2020GL088070, 2020.
- 626 Si, Y. D., Wang, H. M., Cai, K., Chen, L. F., Zhou, Z. C., and Li, S. S.: Long-term (2006-2015) variations and relations
627 of multiple atmospheric pollutants based on multi-remote sensing data over the North China Plain, *Environmental*
628 *Pollution*, 255, 10.1016/j.envpol.2019.113323, 2019.
- 629 Sogacheva, L., Popp, T., Sayer, A. M., Dubovik, O., Garay, M. J., Heckel, A., Hsu, N. C., Jethva, H., Kahn, R. A.,
630 Kolmonen, P., Kosmale, M., de Leeuw, G., Levy, R. C., Litvinov, P., Lyapustin, A., North, P., Torres, O., and Arola,
631 A.: Merging regional and global aerosol optical depth records from major available satellite products, *Atmospheric*
632 *Chemistry and Physics*, 20, 2031-2056, 10.5194/acp-20-2031-2020, 2020.
- 633 Strode, S. A., Worden, H. M., Damon, M., Douglass, A. R., Duncan, B. N., Emmons, L. K., Lamarque, J.-F., Manyin,
634 M., Oman, L. D., Rodriguez, J. M., Strahan, S. E., and Tilmes, S.: Interpreting space-based trends in carbon monoxide
635 with multiple models, *Atmospheric Chemistry and Physics*, 16, 7285-7294, 10.5194/acp-16-7285-2016, 2016.
- 636 Sun, W., Shao, M., Granier, C., Liu, Y., Ye, C. S., and Zheng, J. Y.: Long-Term Trends of Anthropogenic SO₂, NO_x,
637 CO, and NMVOCs Emissions in China, *Earth's Future*, 6, 1112-1133, 10.1029/2018ef000822, 2018.
- 638 United Nations Environment Program (UNEP): Independent Environmental Assessment: Beijing 2008 Olympic
639 Games. Nairobi, Kenya, 2009.
- 640 Wang, M., Zhu, T., Zheng, J., Zhang, R. Y., Zhang, S. Q., Xie, X. X., Han, Y. Q., and Li, Y.: Use of a mobile laboratory
641 to evaluate changes in on-road air pollutants during the Beijing 2008 Summer Olympics, *Atmospheric Chemistry and*
642 *Physics*, 9, 8247-8263, 10.5194/acp-9-8247-2009, 2009.
- 643 Wang, P., Chen, K., Zhu, S., Wang, P., and Zhang, H.: Severe air pollution events not avoided by reduced
644 anthropogenic activities during COVID-19 outbreak, *Resources, Conservation and Recycling*, 158, 104814,
645 10.1016/j.resconrec.2020.104814, 2020.
- 646 Wang, P. C., Elansky, N. F., Timofeev, Y. M., Wang, G. C., Golitsyn, G. S., Makarova, M. V., Rakitin, V. S., Shtabkin,
647 Y., Skorokhod, A. I., Grechko, E. I., Fokeeva, E. V., Safronov, A. N., Ran, L., and Wang, T.: Long-Term Trends of
648 Carbon Monoxide Total Columnar Amount in Urban Areas and Background Regions: Ground- and Satellite-based
649 Spectroscopic Measurements, *Advances in Atmospheric Sciences*, 35, 785-795, 10.1007/s00376-017-6327-8, 2018.
- 650 Wang, T., Nie, W., Gao, J., Xue, L. K., Gao, X. M., Wang, X. F., Qiu, J., Poon, C. N., Meinardi, S., Blake, D., Wang,
651 S. L., Ding, A. J., Chai, F. H., Zhang, Q. Z., and Wang, W. X.: Air quality during the 2008 Beijing Olympics:
652 secondary pollutants and regional impact, *Atmospheric Chemistry and Physics*, 10, 7603-7615, 10.5194/acp-10-7603-
653 2010, 2010.
- 654 Wang, Y., and Wang, J.: Tropospheric SO₂ and NO₂ in 2012-2018: Contrasting views of two sensors (OMI and
655 OMPS) from space, *Atmospheric Environment*, 223, 10.1016/j.atmosenv.2019.117214, 2020.
- 656 Warner, J., Carminati, F., Wei, Z., Lahoz, W., and Attie, J. L.: Tropospheric carbon monoxide variability from AIRS
657 under clear and cloudy conditions, *Atmospheric Chemistry and Physics*, 13, 12469-12479, 10.5194/acp-13-12469-
658 2013, 2013.
- 659 Witte, J. C., Schoeberl, M. R., Douglass, A. R., Gleason, J. F., Krotkov, N. A., Gille, J. C., Pickering, K. E., and
660 Livesey, N.: Satellite observations of changes in air quality during the 2008 Beijing Olympics and Paralympics,
661 *Geophysical Research Letters*, 36, 10.1029/2009gl039236, 2009.

662 Xie, G. Q., Wang, M., Pan, J., and Zhu, Y.: Spatio-temporal variations and trends of MODIS C6.1 Dark Target and
663 Deep Blue merged aerosol optical depth over China during 2000-2017, *Atmospheric Environment*, 214,
664 10.1016/j.atmosenv.2019.116846, 2019.

665 Xu, J. H., Xie, H. M., Wang, K., Wang, J., and Xia, Z. S.: Analyzing the spatial and temporal variations in tropospheric
666 NO₂ column concentrations over China using multisource satellite remote sensing, *Journal of Applied Remote
667 Sensing*, 14, 10.1117/1.jrs.14.014519, 2020.

668 Yu, S. M., Yuan, J. G., and Liang, X. Y.: Trends and Spatiotemporal Patterns of Tropospheric NO₂ over China During
669 2005-2014, *Water Air and Soil Pollution*, 228, 10.1007/s11270-017-3641-9, 2017.

670 Yumimoto, K., Uno, I., and Itahashi, S.: Long-term inverse modeling of Chinese CO emission from satellite
671 observations, *Environmental Pollution*, 195, 308-318, 10.1016/j.envpol.2014.07.026, 2014.

672 Zhang, Y., Li, C., Krotkov, N. A., Joiner, J., Fioletov, V., and McLinden, C.: Continuation of long-term global SO₂
673 pollution monitoring from OMI to OMPS, *Atmospheric Measurement Techniques*, 10, 10.5194/amt-10-1495-2017,
674 2017.

675 Zhao, Y., Nielsen, C. P., McElroy, M. B., Zhang, L., and Zhang, J.: CO emissions in China: Uncertainties and
676 implications of improved energy efficiency and emission control, *Atmospheric Environment*, 49, 103-113,
677 10.1016/j.atmosenv.2011.12.015, 2012.

678 Zhao, Y., Zhang, J., and Nielsen, C. P.: The effects of recent control policies on trends in emissions of anthropogenic
679 atmospheric pollutants and CO₂ in China, *Atmospheric Chemistry and Physics*, 13, 487-508, 10.5194/acp-13-487-
680 2013, 2013.

681 Zheng, B., Chevallier, F., Ciais, P., Yin, Y., Deeter, M. N., Worden, H. M., Wang, Y. L., Zhang, Q., and He, K. B.:
682 Rapid decline in carbon monoxide emissions and export from East Asia between years 2005 and 2016, *Environmental
683 Research Letters*, 13, 10.1088/1748-9326/aab2b3, 2018a.

684 Zheng, B., Tong, D., Li, M., Liu, F., Hong, C. P., Geng, G. N., Li, H. Y., Li, X., Peng, L. Q., Qi, J., Yan, L., Zhang,
685 Y. X., Zhao, H. Y., Zheng, Y. X., He, K. B., and Zhang, Q.: Trends in China's anthropogenic emissions since 2010 as
686 the consequence of clean air actions, *Atmospheric Chemistry and Physics*, 18, 14095-14111, 10.5194/acp-18-14095-
687 2018, 2018b.

688

689 **Tables**

690

691 **Table 1. Summary statistics for central east China comparing 2020 and 2019 during January 23 – April 8.**

Variable	2020 mean	2019 mean	2020 % difference from 2019
CO (ppbv)	133.5 (130.3, 136.8)	137.9 (134.7, 141.3)	-3.2 (-6.3, 0.1)
SO₂ (DU)	0.057 (0.045, 0.070)	0.031 (0.018, 0.046)	95 (14.8, 249.6)
NO₂ (10 ¹⁵ molec cm ⁻²)	6.5 (5.8, 7.2)	9.6 (8.7, 10.5)	-32.1 (-42.1, -21.7)
AOD	0.41 (0.36, 0.46)	0.48 (0.41, 0.55)	-14.3 (-29.4, 3.1)

692

693

694 **Table 2. Same as Table 1, but for southern China.**

Variable	2020 mean	2019 mean	2020 % difference from 2019
CO (ppbv)	144.7 (139.6, 150.3)	128.5 (124.4, 132.8)	12.6 (7.2, 18.3)
SO₂ (DU)	0.003 (-0.01, 0.020)	-0.020 (-0.04, -0.001)	116 (24, 223)
NO₂ (10 ¹⁵ molec cm ⁻²)	3.3 (3.0, 3.7)	4.3 (3.9, 4.7)	-22.2 (-32.6, -10.4)
AOD	0.38 (0.34, 0.43)	0.34 (0.30, 0.39)	12 (-7, 34)

695

696 **Table 3. 2014 anthropogenic emissions estimates by sector (in %) over China, excluding biomass burning, from the**
 697 **Community Emissions Data System (CEDs) for a representative set of constituents: black carbon (BC), carbon monoxide**
 698 **(CO), ammonia (NH₃), nitrogen oxides (NO_x), organic carbon (OC) and sulfur dioxide (SO₂). Residential, commercial and**
 699 **other sectors are combined as RCO.**

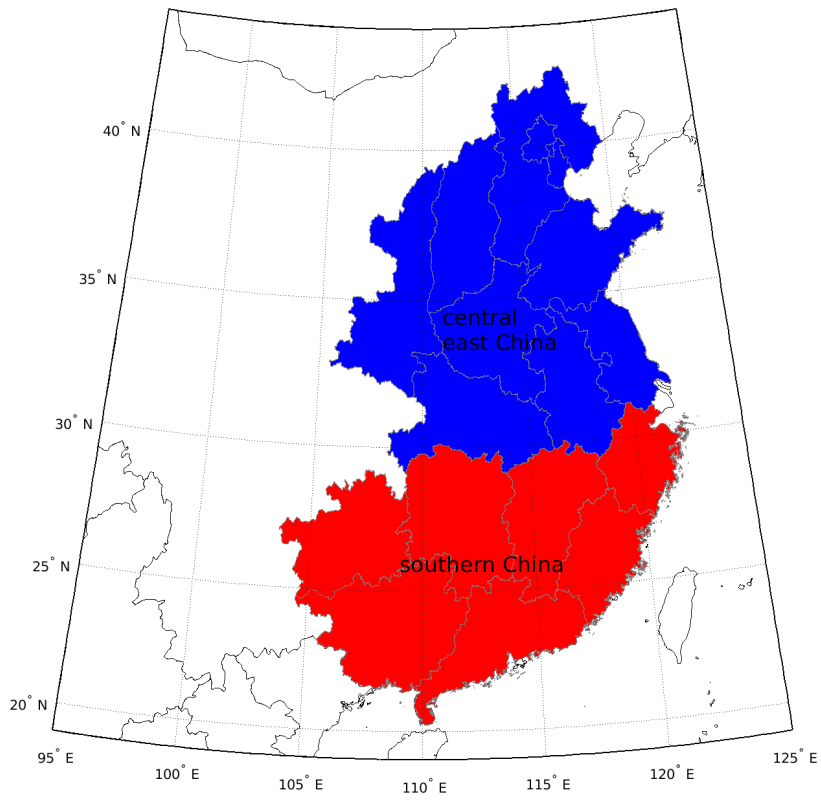
	BC	CO	NH₃	NO_x	OC	SO₂
Agriculture	0	0	61.6	1.1	0	0
Energy	32.6	8	0.4	38.5	28.3	29.4
Industrial	12.7	41.8	6.5	33	5.1	57.3
Ground transportation	8.1	7.2	0.5	17.5	1.7	0.3
RCO	38.1	36.7	5.2	4.2	38.4	12.5
Solvents	0	0	0	0	0	0
Waste	8.5	6.3	25.8	5.2	26.5	0.4
Shipping	0	0	0	0.2	0	0.1
Aircraft	0	0	0	0.2	0	0

700

701 **Table 4. Bottom up biomass Global Fire Assimilation System (Kaiser et al., 2012) burning CO emissions estimates from the**
 702 **Upper Mekong region (17° N to 24° N, 95° E to 105° E) and AIRS CO over southern China from January 23 to April 8, for**
 703 **2005-2020.**

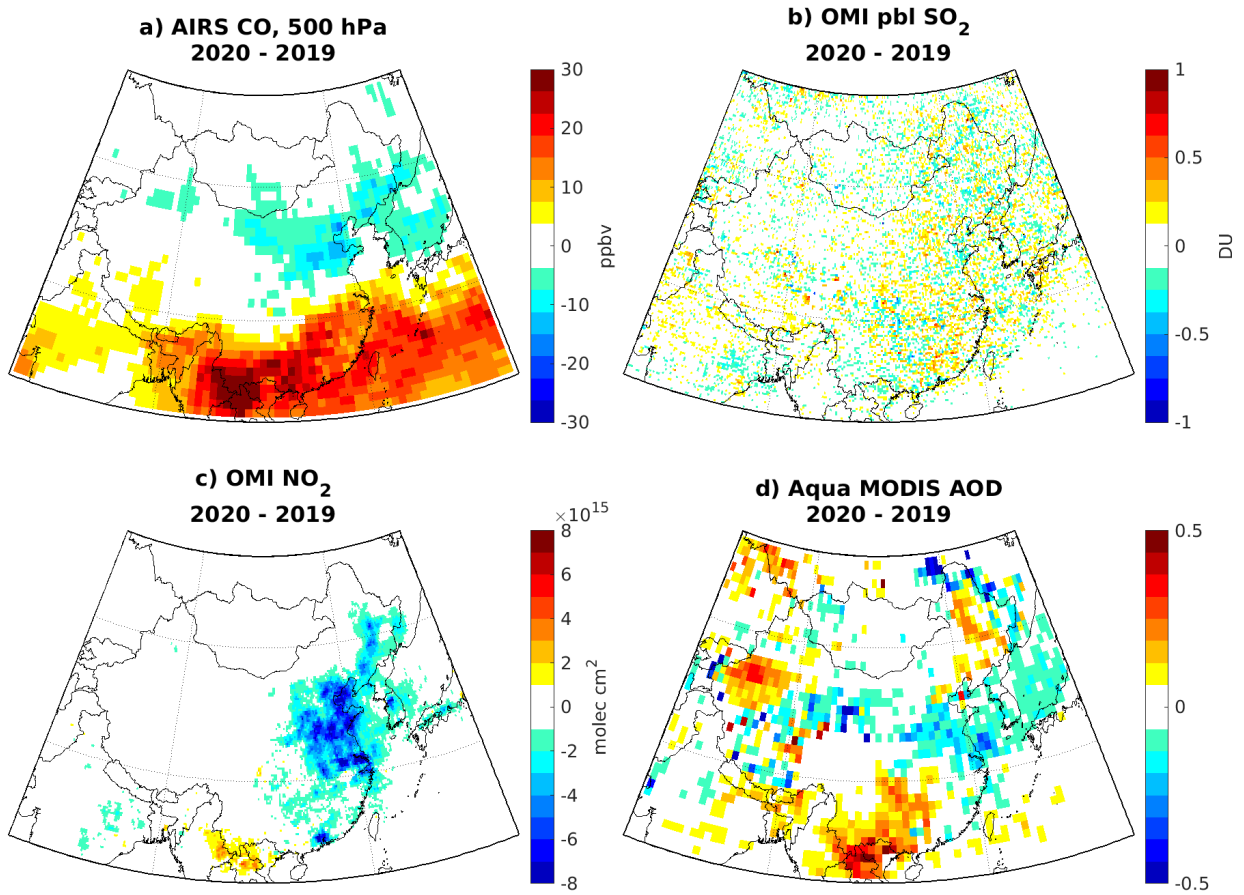
Year	GFAS CO	AIRS CO
	Upper Mekong (KT)	southern China 500 hPa (ppbv)
2005	7977	157
2006	8905	146
2007	15734	165
2008	4542	153
2009	9990	140
2010	14176	149
2011	3591	147
2012	11320	153
2013	8684	145
2014	8722	142
2015	8084	143
2016	9642	149
2017	3736	131
2018	3179	139
2019	6309	128
2020	7871	145

704



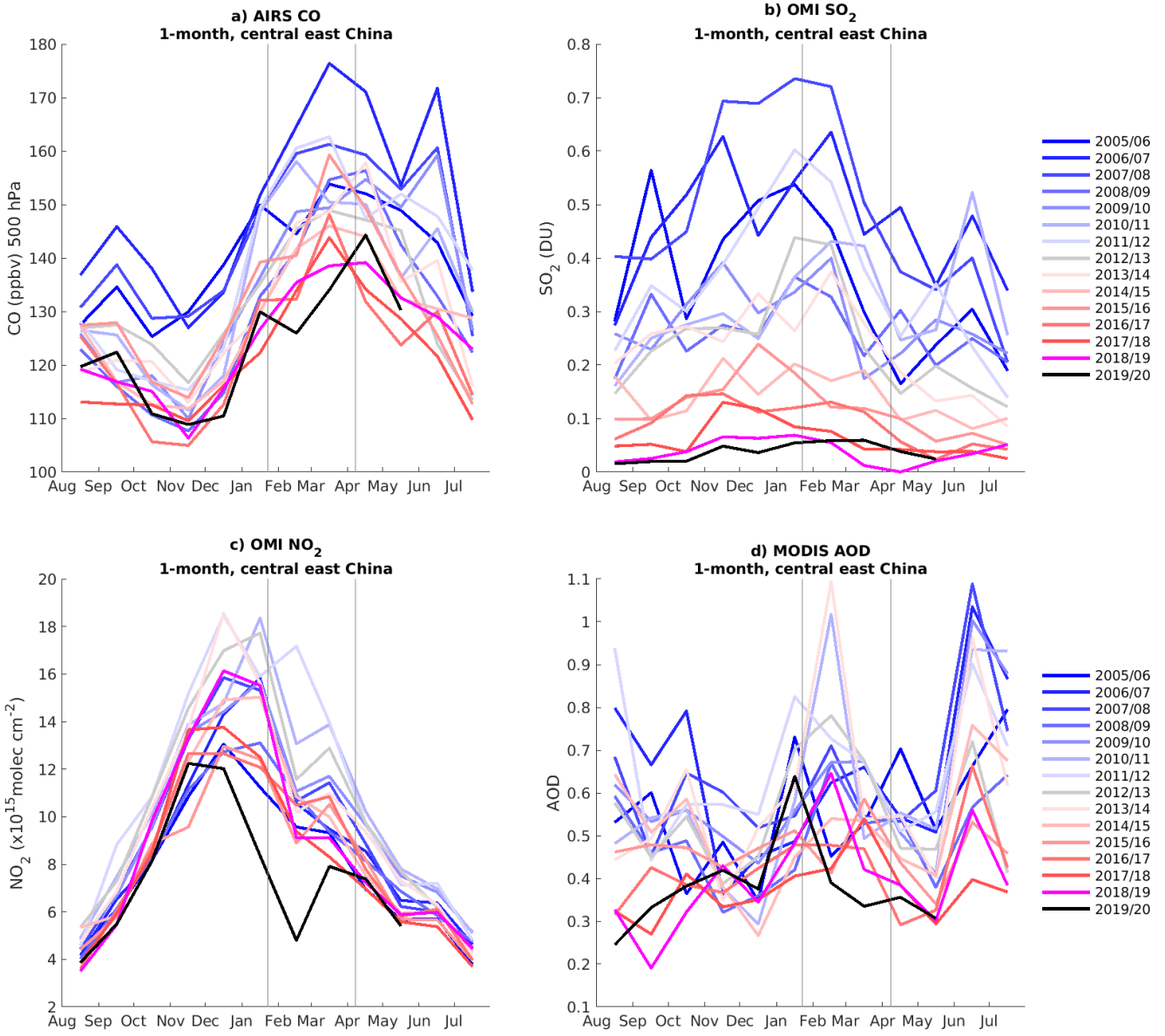
706

707 **Figure 1. Groupings of provinces for central east China and southern China.**



708

709 **Figure 2. 2020-2019 differences during January 23 to April 8 over China in a) AIRS carbon monoxide (CO) at 500 hPa, b)**
 710 **OMI PBL sulfur dioxide (SO₂), c) OMI tropospheric nitrogen dioxide (NO₂) and d) Aqua MODIS aerosol optical depth**
 711 **(AOD).**



715 **Figure 3. Monthly mean a) AIRS CO, b) OMI PBL SO₂, c) OMI tropospheric NO₂ and d) MODIS AOD over central east China since 2005. As in Bauwens et al. (2020), each year starts in August to show any departure from the seasonal cycle during the January 23 to April 8 lockdown period, shown by the thin grey vertical lines.**

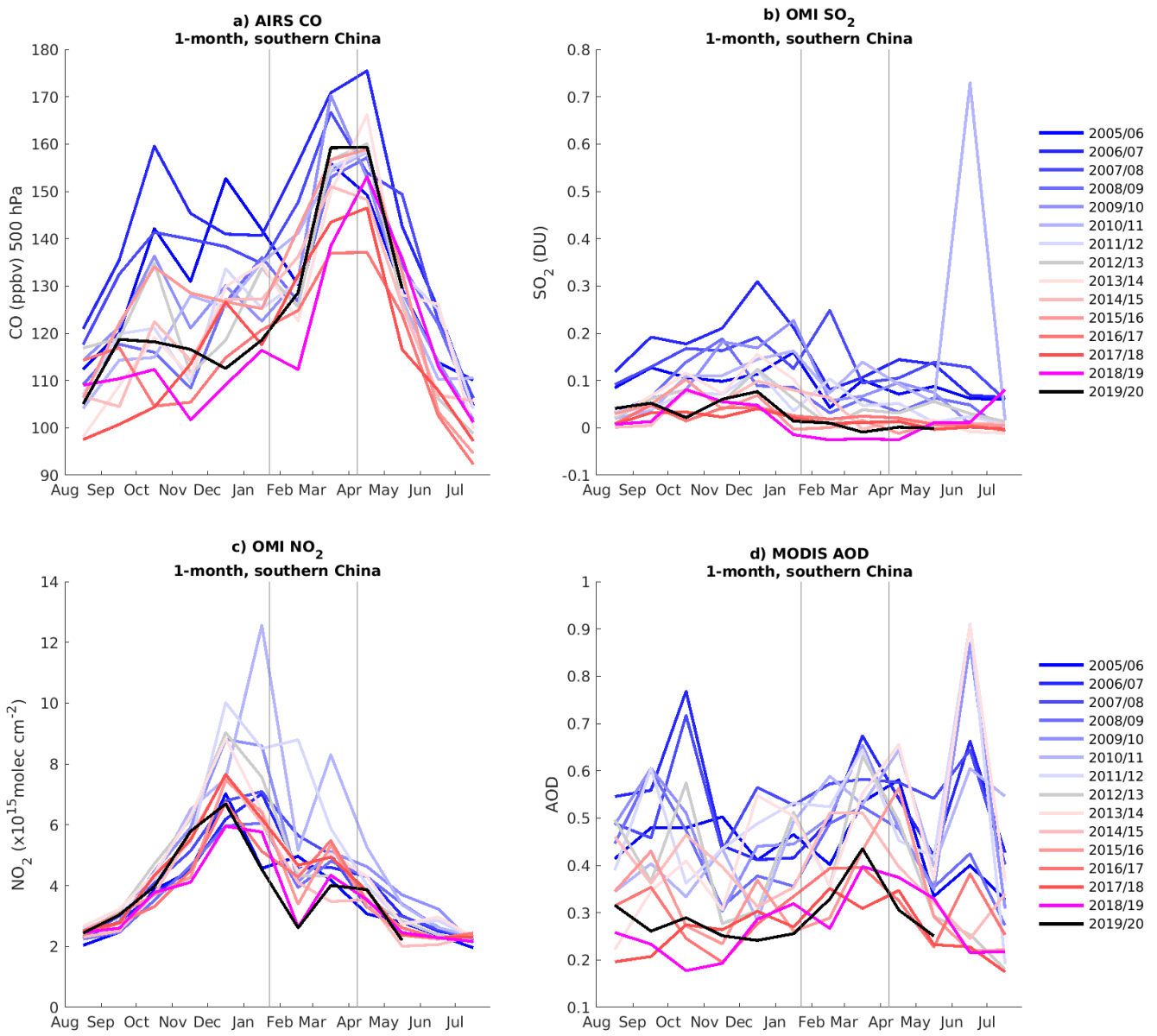
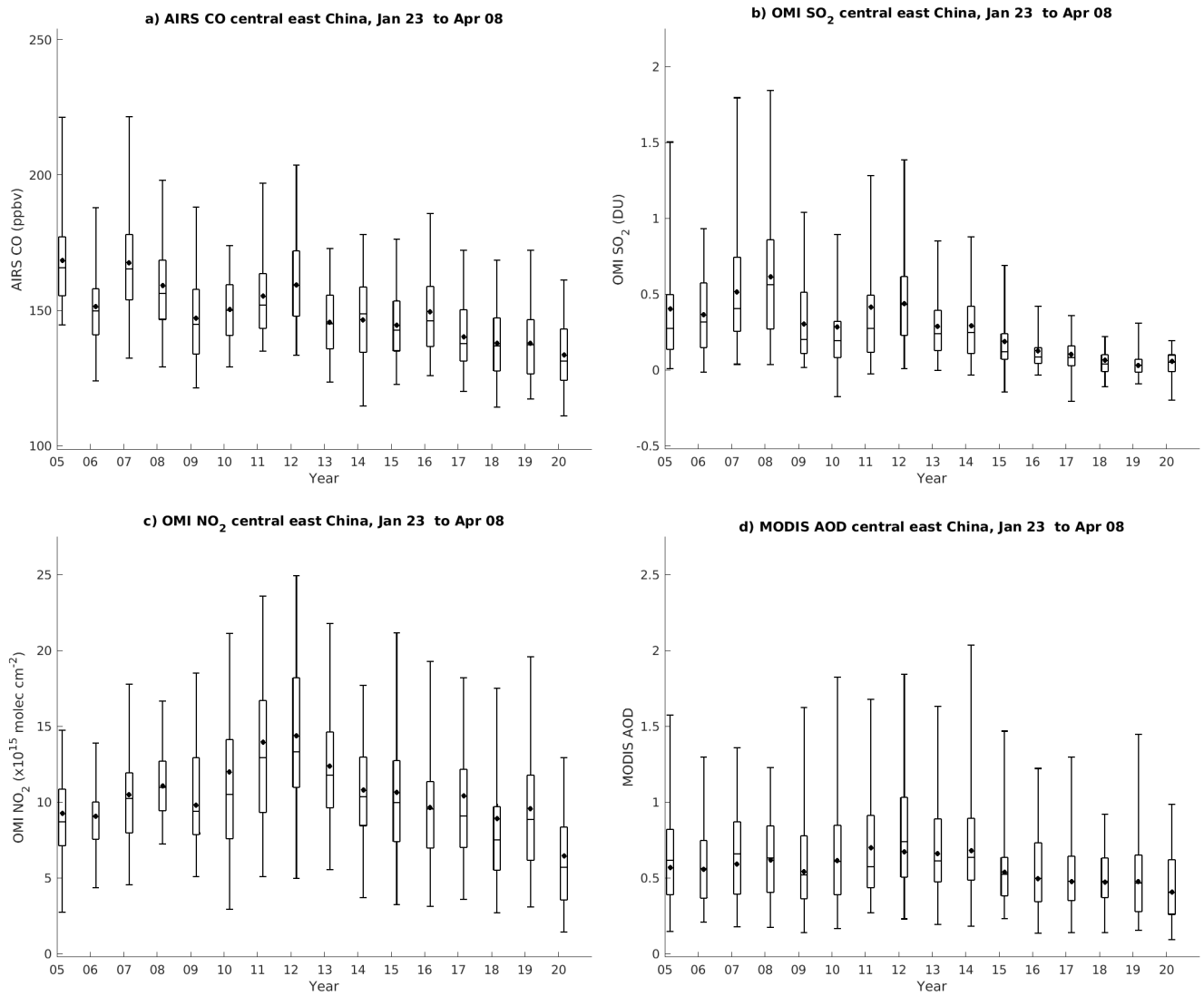
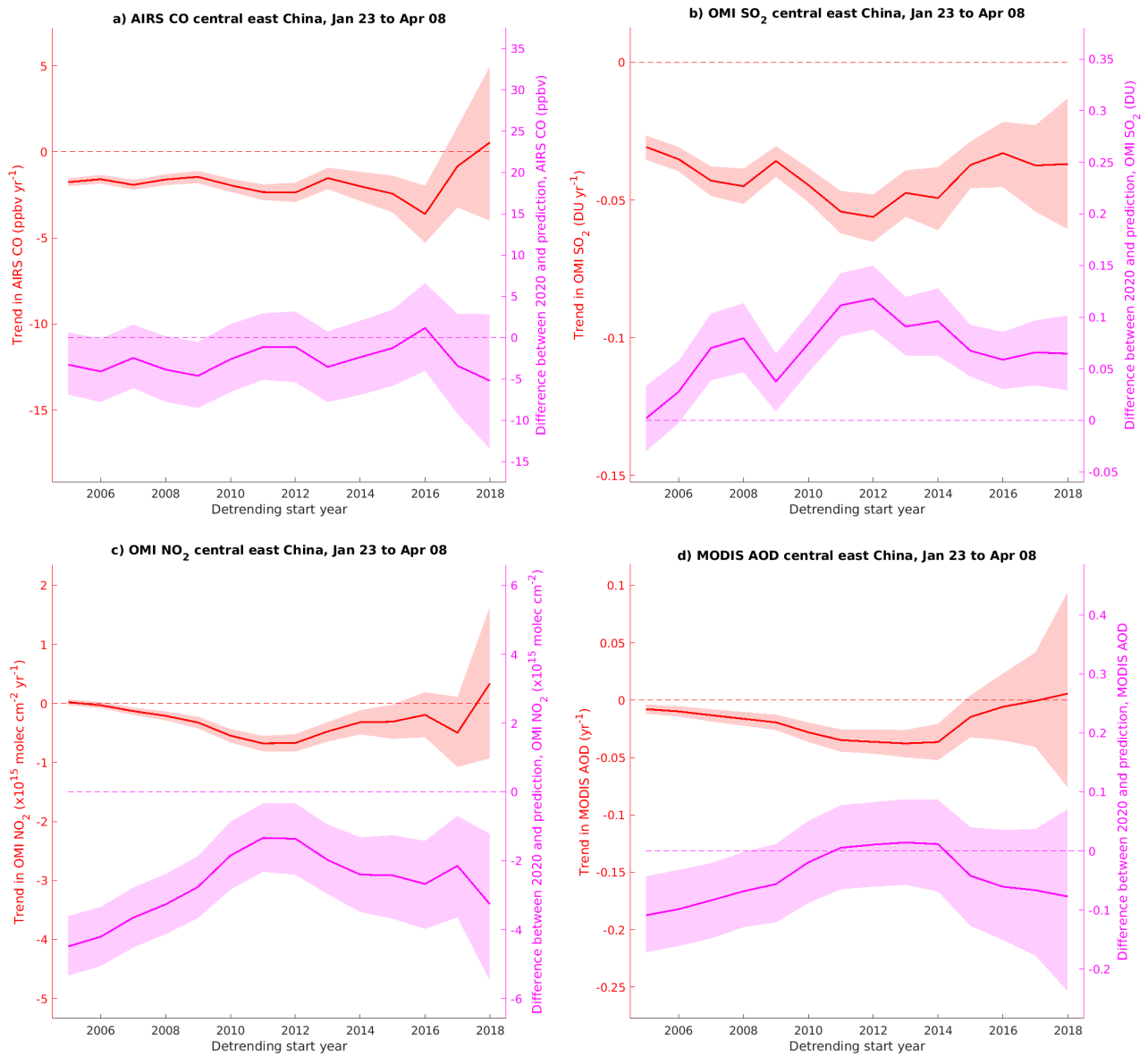


Figure 4. Same as [Figure 3](#), but for southern China.



720 **Figure 5. January 23-April 8 box plots over central East China for a) AIRS CO, b) OMI PBL SO₂, c) OMI tropospheric NO₂ and d) Aqua and Terra MODIS AOD from 2005 to 2020. The black box plots show the median, interquartile range and 2.5th and 97.5th percentiles over all daily data, with the mean shown by the black dot.**



725 **Figure 6. Dependence of trends (red) and difference between 2020 observations and predicted value (magenta) on detrending start year over central east China for a) AIRS CO, b) OMI PBL SO₂, c) OMI tropospheric NO₂ and d) MODIS AOD. The solid line shows the mean of the estimate for each year and the shading shows the 95% confidence interval.**

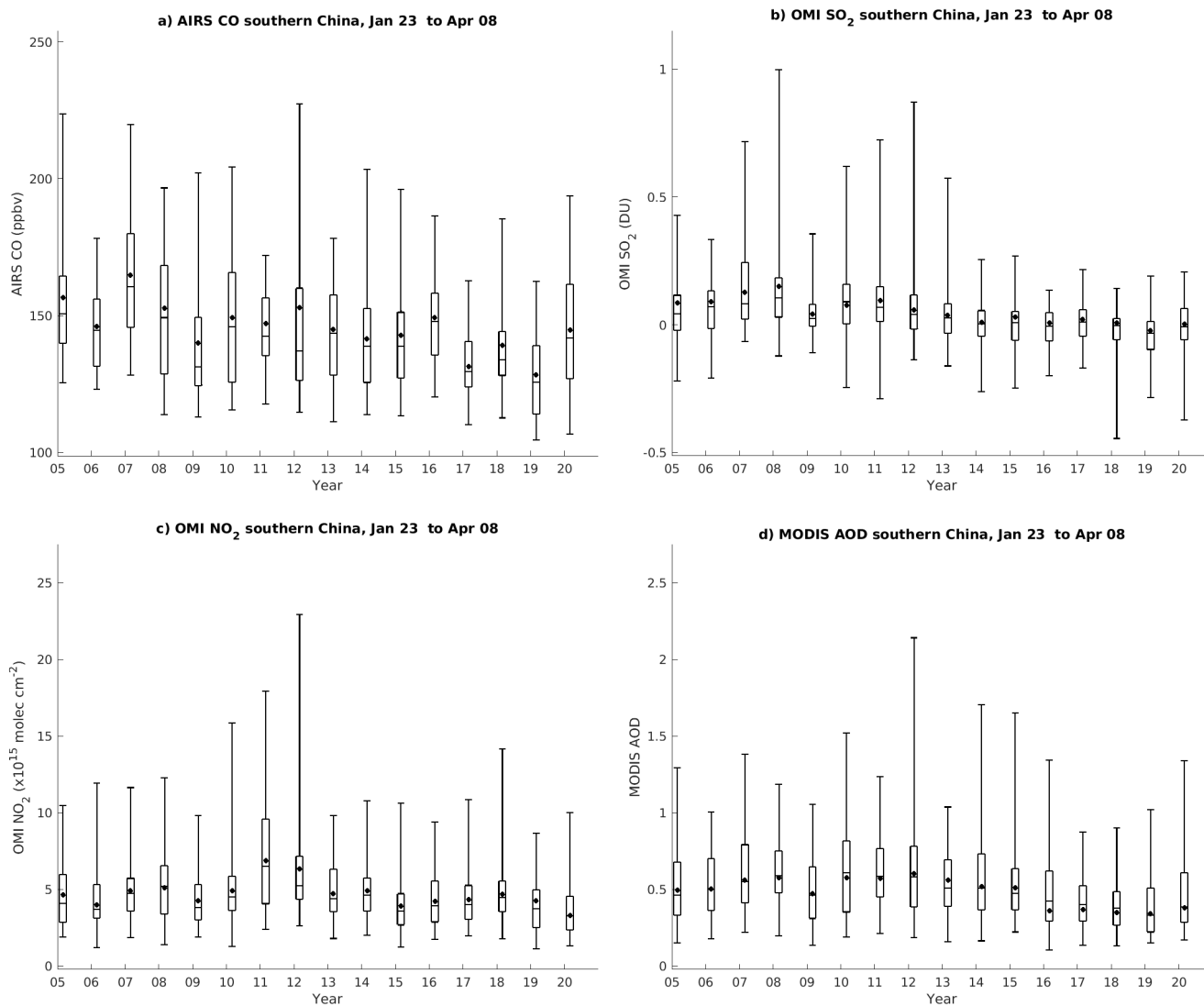
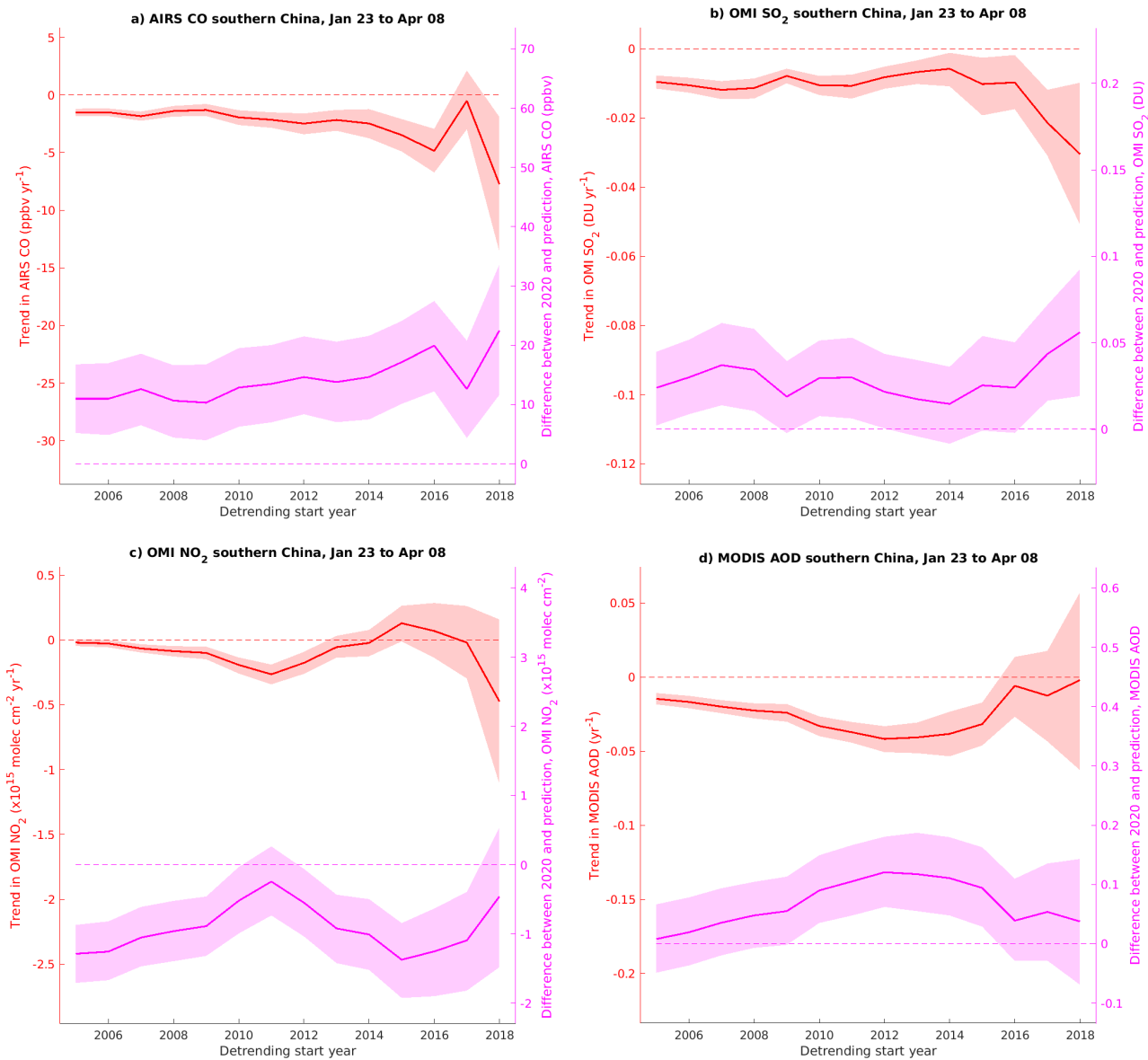


Figure 7. Same as Figure 5 but for southern China.



730 **Figure 8.** Same as Figure 6, but for southern China.